Nat. Hazards Earth Syst. Sci. Discuss., https://doi.org/10.5194/nhess-2017-425
Manuscript under review for journal Nat. Hazards Earth Syst. Sci.
Discussion started: 2 January 2018

Natural Hazards and Earth System Sciences
Discussions

Regional physically based landslide early warning modelling: soil parameterisation and validation of the results

Teresa Salvatici[1], Veronica Tofani[1], Guglielmo Rossi[1], Michele D'Ambrosio[1], Carlo Tacconi Stefanelli[1], Elena Benedetta Masi[1], Ascanio Rosi[1], Veronica Pazzi[1], Pietro Vannoci[1], Miriana Petrolo[1], Filippo Catani[1], Sara Ratto[2], Hervè Stevenin[2] and Nicola Casagli[1]

[1]Department of Earth Sciences, University of Firenze, Firenze, 50121, Italy
[2]Centro funzionale, Regione Autonoma Valle d'Aosta, Aosta, 11100, Italy

Correspondence to: Michele D'Ambrosio (michele.dambrosio@unifi.it)

Abstract.

In this work, we apply a physically-based model, namely the HIRESSS (High REsolution Stability Simulator) model, to forecast the occurrence of shallow landslides at regional scale. The final aim is the set-up of an early warning system at regional scale for shallow landslides. HIRESSS is a physically based distributed slope stability simulator for analysing shallow landslide triggering conditions in real time and in large areas using parallel computational techniques. The software can run in real-time by assimilating weather data and uses Monte Carlo simulation techniques to manage the geotechnical and hydrological input parameters. The test area is a portion of the Valle d'Aosta region, located in North-West Alpine mountain chain. The geomorphology of the region is characterized by steep slopes with elevations ranging from 400 m a.s.l of Dora Baltea's river floodplain to 4810 m a.s.l. of Mont Blanc. In the study area, the mean annual precipitation is about 800-900 mm. These features lead to a high hydrogeological hazard in the whole territory, as mass movements interest the 70% of the municipality areas (mainly shallow rapid landslides and rock falls). In order to apply the model and to increase its reliability, an in-depth study of the geotechnical and hydrological properties of hillslopes controlling shallow landslides formation was conducted. In particular, two campaigns of on site measurements and laboratory experiments were performed with 12 survey points. The data collected contributes to generate input map of parameters for HIRESSS model. In order to take into account the effect of vegetation on slope stability, the contribution of the root cohesion has been also taken into account based on the vegetation map and literature values. The model was applied in back analysis on two past events that have affected Valle d'Aosta region between 2008 and 2009, triggering several fast shallow landslides. The validation of the results, carried out using a database of past landslides, has provided good results and a good prediction accuracy of the HIRESSS model both from temporal and spatial point of view. A statistical analysis of the HIRESSS outputs in terms of failure probability has been carried out in order to define reliable alert levels for regional landslide early warning systems.

Nat. Hazards Earth Syst. Sci. Discuss., https://doi.org/10.5194/nhess-2017-425
Manuscript under review for journal Nat. Hazards Earth Syst. Sci.
Discussion started: 2 January 2018

Natural Hazards and Earth System Sciences
Discussions

1 Introduction

A landslide early warning system is defined as the set of capacities needed to generate and disseminate timely and meaningful warning information to enable individuals, communities and organizations threatened by hazards to prepare and act appropriately and in sufficient time to reduce the possibility of harm or loss (UNISDR, 2009). Warning systems for landslides can be designed and employed at different reference scales. Two categories of early warning systems can be defined on the basis of their scale of analysis: local systems for single slopes (Intrieri et al., 2013) and regional systems. Regional early warning systems for shallow landslides can be developed following two approaches: a) rainfall thresholds based on statistical analysis of rainfall and landslides and b) physically-based deterministic models. While the first approach is currently extensively used at regional scale (Aleotti, 2004; Cannon et al., 2011; Martelloni et al., 2012; Rosi et al., 2012; Lagomarsino et al., 2013), the latter is more frequently applied at slope or catchment scale (Dietrich and Montgomery 1998; Pack et al. 2001; Baum et al. 2002, 2010; Lu and Godt 2008; Simoni et al. 2008; Ren et al. 2010; Arnone et al. 2011; Salciarini et al., 2012; Park et al., 2013; Rossi et al. 2013; Salciarini et al. 2017). This is because the poor knowledge of hydrological and geotechnical parameters spatial distribution, caused by the extreme heterogeneity and inherent variability of soil at large scale (Mercogliano et al., 2013; Tofani et al., 2017), mainly avoid the physically-based model application at regional scale.

Moreover, in the physically based modelling the effect of vegetation in terms of roots reinforcement has to be taken into account on slopes stability since it plays a crucial role (Gray and Magahan, 1981). Mainly through the root systems, in fact, vegetation strongly affects the mechanical and hydrological soil behaviour, and in particularly the shallow landslides triggering processes. Except for particular contexts, the vegetation constitutes a mitigating element for the instability (Chirico et al. 2013). The stabilizing action of the vegetal communities in the slopes vadose zone is mainly due to reinforcement of the soil by the root network (increase of the tensile strength) (Gray and Sotir, 1996; Vergani et al., 2017).

In this work, we apply the physically based model, named HIRESSS (Rossi et al., 2013) in Eastern part of Valle d'Aosta region (Italy), in North-West Alpine mountain chain to forecast the occurrence of shallow landslides at regional scale. HIRESSS is a physically based distributed slope stability simulator for analysing shallow landslide triggering conditions in real time and in large areas using parallel computational techniques. In the area selected, an in-depth study of the geotechnical and hydrological properties of hillslopes controlling shallow landslides formation was conducted, performing two campaigns (12 survey points) of in-situ measurements and laboratory tests. Furthermore, the HIRESSS model has been modified to take into account the effect of the root reinforcement to the stability of slopes based on the vegetation map and literature values.

The HIRESSS model simulated two past events, one in 2008 and one in 2009, and the validation of the model performance was carried out comparing the results with the landslide regional database.

In particular:

- 24 - 31 May 2008: on 28 and 29 May 2008 intense and persistent rainfall was recorded across the Valle d'Aosta region with a total precipitation in the study area of about 250 mm causing flooding, debris flows and rockfalls.
- 25 - 28 April 2009: from 26 April to 28 April 2009 heavy rainfall affected the south-eastern part of the Valle d'Aosta region, with the highest precipitation recorded at the Lillianes Granges station of about 268 mm. This precipitation triggered several landslides.

Eventually, a discussion on how the model results can be analysed in order to set up an early warning system is provided.

2 Study area

The study area, called alert Zone B by the regional civil protection authorities, is located in eastern part of Valle d'Aosta region, in North-West Alpine mountain chain (Fig. 1). The area is characterized by three main valleys: Champorcher valley, Gressoney or Lys valley, and Ayas valley. The first is located on the right side of Dora Baltea water catchment, and represent the southern part of the study area. The second and third valleys show N-S orientation, and they are delimited to north by Monte Rosa massif (4527 m a.s.l) and to south by Dora Baltea river. The geomorphology of the region is characterized by steep slopes, high climatic and altitude (ranging from 400 m a.s.l of Dora Baltea's river floodplain to 4810 m a.s.l. of Mont Blanc) variability. From a geomorphologic point of view, valleys shaped by glaciers characterize the territory. The glacial modelling is shown in the U-shaped of Lys and Ayas valleys, and the erosive depositional forms found in the Ayas valley. The three valleys' watercourses, the Lys creek, the Evançon creek, and the Dora Baltea river, contributed to the glacial deposits modelling with the formation of alluvial fans

From a geological point of view, the Valle d'Aosta is located NW with respect to the Insubrica Line, in particular, there are three systems of Europa chain: the Austroalpino, the Pennidiche, and the Elvetico-Ultraelevato systems (De Giusti, 2004). Fig. 2 shows the lithological map of the study area (alert Zone B) obtained by reclassifying the geological units according to 8 lithological group: landslides, alluvial deposits, glacial deposits, colluvial deposits, Calcareous schist, Granites, Mica schists, Pietre Verdi. In detail in the study area the main lithologies outcropping are metamorphic and intrusive rocks, in particular granites, metagranites, schists and serpentinite.

The slope steepness, together with mean annual precipitation of 800-900 mm are the main landslide triggering factors. These features lead to a high hydrogeological hazard in the whole territory, in particular mass movements interest the 70% of the municipality areas, as: rock falls, Deep Seated Gravitational Slope Deformations (DSGSD), debris avalanches, debris flow, and debris slide.

Nat. Hazards Earth Syst. Sci. Discuss., https://doi.org/10.5194/nhess-2017-425
Manuscript under review for journal Nat. Hazards Earth Syst. Sci.
Discussion started: 2 January 2018

Natural Hazards and Earth System Sciences Discussions

3 Methodology

3.1 Soil Geotechnical and hydrological characterization

The properties of slope deposits were determined by in situ and laboratory measurements (Bicocchi et al., 2016; Tofani et al., 2017) at 12 survey points. To carry out the in situ tests the survey points were selected following these characteristics: i) physiography, ii) landslides occurrence, and iii) geo-lithology (Fig. 2). Regarding the first point, a high-resolution DEM (from Val d'Aosta Regional Authorities) was used to locate the most suitable slopes. The surveys took place in two sessions, the first one in August 2016, and the second one in September 2016. The following analyses were conducted:

- registration of geographical position using a GPS and photographic documentation of the site characteristics (morphology and vegetation);
- in situ measurement of saturated hydraulic conductivity (k_s) by means of the constant-head well permeameter Amoozemeter;
- sampling of an aliquot (~2 kg each) of the material for laboratory tests, including grain size distributions, index properties, Atterberg limits and direct shear tests.

The permeability in-situ measurements and the soil samplings were made at depth ranging from 0.4 to 0.6 m below the ground level. The evaluation of the k_s (saturated hydraulic conductivity or permeability) was made with the *Amoozemeter* permeameter (Amoozegar, 1989). The measurement was obtained by observing the amount of water required to maintain a constant volume of water into the hole. In situ measurements are then applied into the Glover solution (Eq. 1), which calculates the saturated permeability of the soils:

$$k_s = \frac{Q\left[\sinh^{-1}\left(\frac{h}{r}\right) - \left(\frac{r^2}{h^2}+1\right)^{\frac{1}{2}} + \frac{r}{h}\right]}{2\pi h^2} \quad (1)$$

where Q is the steady-state rate of water flow from the permeameter into the auger hole, h is the water depth in the borehole (constant), and r is the borehole radius. The k_s is a very useful parameter not only for slope stability modelling but also for many other hydrological problems (groundwater, surface water runoff and sub-surface, flow calculation of water courses).

In addition, the in situ collected samples were examined in the laboratory to define a wide range of parameters to characterize more extensively the deposits. In particular, the following tests were performed in order to classify the analysed soils:

- grain size distribution (determination of granulometric curve for sieving and settling following ASTM recommendations), and classification of soils (according to AGI and USCS classification, Wagner, 1957);
- determination of the main index properties (porosity, relationships of phases, natural water content w_n, natural and dry unit weight γ and γ_d) following the ASTM recommendations;
- determination of Atterberg limits (liquid limit LL, plastic limit PL, and plasticity index PI);
- direct shear test on selected samples.

Based on the result obtained from the granulometric tests, the analysed soils are predominantly sands with silty gravel (Fig. 3 and Table 1).

Regarding the index properties, the natural soil water content values were predominantly about 20% by weight, with a maximum and minimum values of 5.1% and 26.2%, respectively. These values reflect their different ability to hold water in their voids. The measured natural unit weight (γ) was variable between 15.3 kN/m^3 and 21.7 kN/m^3, depending not only on the different grain size distribution but also of different thickening and consolidation states. Regarding saturated unit weight (γ_{sat}) the measured values range between 18.2 kN/m^3 and 21.5 kN/m^3 (Table 1).

The Atterberg limits (LL and PL) were measured on samples with a sufficient passing fraction (> 30% by weight) through 40 ASTM (0.425 mm) sieve. For sandy prevalent samples, LL values are predominantly around 40% of water content (% by weight), while the PL is around 30% (Table 1).

The effective friction angle varies between a minimum of 25.6° and a maximum of 34.3°, while the effective cohesion ranges from a minimum of 0.0 kPa to a maximum of 9.3 kPa. Consistent with the presence of sandy soils, the saturated permeability values were around a medium-high value of 10^{-6} m/s. The minimum and maximum values were found between $1.36 \cdot 10^{-7}$ m/s and $1.54 \cdot 10^{-5}$ m/s. Considering the poor variability of samples, the permeability values were relatively homogeneous and in accordance with the values reported in the literature (Table 1).

3.2. Evaluation of root reinforcement

Root reinforcement is due to root tensile strength that is usually greater than the tensile strength of soil. Conversely, soil has a greater strength to compression, therefore the overall effect is a strengthened matrix soil, in which stresses are relocated from sediments to roots (Greenway, 1987). Consequently, the strength of rooted soil results from sediments nature (cohesion and friction angle), root strength and strength of soil-roots bonds (Waldron, 1977; Waldron and Dakessian, 1981; Ennos, 1990). Regarding strength parameters, roots seem to affect the cohesion parameter only, while the friction angle would be poorly or not at all interested by reinforcement (Waldron and Dakessian, 1981; Gray and Ohashi 1983; Operstein and Frydaman, 2000; Giadrossich et al., 2010). Most commonly used models to quantify rooted soils strength are based on a Mohr-Coulomb failure criterion for unsaturated soil in which a term representing root reinforcement is added (Eq. 2):

$$\tau = c' + (\mu_a - \mu_w)\tan\varphi_b + (\sigma - \mu_a)\tan\varphi' + c_r \quad (2)$$

where τ is the soil-shearing resistance, c' effective cohesion, μ_a the pore-air pressure, μ_w the pore-water pressure, φ_b the angle describing the increase in shear strength due to an increase in matric suction (μ_a - μ_w), σ the normal stress on the shear plane, φ' the effective soil friction angle, and c_r the increase in shear strength due to roots. The root reinforcement (or root cohesion) can be considered equal to (Eq. 3):

$$c_r = kT_r(A_r/A) \quad (3)$$

where T_r is the root failure strength (tensile, frictional, or compressive) of roots per unit area of soil, A_r/A the root area ratio (proportion of area occupied by roots per unit area of soil), k a coefficient dependent on the effective soil friction angle and the orientation of roots. The measure of cr varies with vegetal species, within a single species depends on how plants respond to environmental characteristics and fluctuations.

In view of all that has been mentioned so far, it is necessary to consider the root cohesion in calculating FS and consequently in applying HIRESSS model. The additional cohesion induced by roots assumes different values not only depending on plant species and environmental characteristics, but also on depth of soil, as roots diameter and density vary with latter. Because of such evidence, studies on roots cohesion of different species report values as function of depth of soil. In the area of the case study, soils have thinner thickness than those ones in which such studies are carried out. In such thin soils, root systems organize their growth depending on available space not reaching the same depth of roots of thick soils. Consequently, in this context root cohesion of species at the different depth is dissimilar related to literature values. Considering this, map for variation of root cohesion is processed taking for each species the minimum cohesion (among those specified for each species at the different depth) reported in literature. By doing this, contribution of vegetation to stability of slopes is considered in FS calculate and at the same time, it is avoided an overestimate of root cohesion.

In the area, root cohesion defined as mentioned above ranges from a minimum of 0.0 kPa (mainly in the outcrop area, to maximum of 8.9 kPa (in the area occupied by mountain maple situated on the left bank of river Dora Baltea).

3.3 HIRESSS description

The physically-based distributed slope stability simulator HIRESSS (Rossi et al., 2013) is a model developed to analyse shallow landslide triggering conditions on large scale at high spatial and temporal resolution using parallel calculation method. Two parts compose the model: hydrological and geotechnical (Rossi et al., 2013). The hydrological part is based on a dynamical input of the rainfall data which are used to calculate the pressure head and provide it to the geotechnical stability model. The hydrological model is initiated as a modelled form of hydraulic diffusivity, using an analytical solution of an approximated form of the Richards equation under the wet condition (Richards, 1931). The equation solution allows us to calculate the pressure head variation (h), depending on time (t) and depth of the soil (Z). The solutions are obtained by imposing some boundary conditions as described by Rossi et al. (2013).

The geotechnical stability model is based on an infinite slope stability model. The model considers the effect of matric suction in unsaturated soils, taking into account the increase in strength and cohesion. The stability of slope at different depths (Z values) is computed since the hydrological model calculates the pressure head at different depths. The variation of soil mass caused by water infiltration on partially saturated soil is also modelled. The original FS equations (Rossi et al., 2013) were modified taking into account the effect of root reinforcement (c_r) as an increase of soil cohesion (c') according to the Eq. 4:

$$c_{tot} = c' + c_r \quad (4)$$

The new equation of FS at unsaturated conditions is therefore (Eq. 5):

Nat. Hazards Earth Syst. Sci. Discuss., https://doi.org/10.5194/nhess-2017-425
Manuscript under review for journal Nat. Hazards Earth Syst. Sci.
Discussion started: 2 January 2018

$$FS = \frac{\tan\varphi}{\tan\alpha} + \frac{c_{tot}}{\gamma_d y \sin\alpha} + \frac{\gamma_w h \tan\varphi\left\{\left[1+\left(h_b^{-1}|h|\right)^{\lambda+1}\right]^{\frac{\lambda}{\lambda+1}}\right\}^{-1}}{\gamma_d y \sin\alpha} \quad (5)$$

where φ is the friction angle, α is the slope angle, γ_d is the dry soil unit weight, y is the depth, γ_w is the water unit weight, h is the pressure head, h_b is the bubbling pressure, and λ is the pore size index distribution. In saturated condition the equation of FS (Rossi et al., 2013) becomes (Eq. 6):

$$FS = \frac{\tan\varphi}{\tan\alpha} + \frac{c_{tot}}{(\gamma_d(y-h)+\gamma_{sat}h)\sin\alpha} - \frac{\gamma_w h \tan\varphi}{(\gamma_d(y-h)+\gamma_{sat}h)\tan\alpha} \quad (6)$$

where γ_{sat} is the saturated soil unit weight.

One of the major problems, associated with the deterministic approach employed on a large scale, is the uncertainty of the static input parameters or geotechnical parameters of the soil. The method used for the estimation of parameters spatial variability is the Monte Carlo Simulation. The Monte Carlo simulation achieves a probability distribution of input parameters providing results in terms of slope failure probability. The developed software uses the computational power offered by multicore and multiprocessor hardware, from modern workstations to supercomputing facilities (HPC), to achieve the simulation in reasonable runtimes, compatible with civil protection real time monitoring (Rossi et al. 2013).

3.4 HIRESSS input data

The HIRESSS model loads spatially distributed data arranged as input raster maps. Therefore, point data and parameters have to be adequately spatially distributed. In this application the spatial resolution was 10 m and 12 raster maps of static input parameters were prepared. These input raster were (Fig. 4): slope gradient; effective cohesion (c'); root cohesion (c_r); friction angle (φ'); dry unit weight (γ_d); soil thickness; hydraulic conductivity (k_s); initial soil saturation (S); pore size index (l); bubbling pressure (h_s); effective porosity (n); and residual water content (q_r).

The slope gradient (Fig. 5a) was calculated from the DEM (Digital Elevation Model). Effective cohesion, friction angle (Fig. 5b), hydraulic conductivity (Fig. 5c), effective porosity (Fig. 5f) and dry unit weight (Fig. 5g), were obtained, spatializing according to lithology, the soil punctual parameters derived from the in situ and laboratory geotechnical tests and analysis carried out as described in sect. 3.1. Soil thickness (Fig. 5e) was calculated by the GIST model (Catani et al., 2010; Del Soldato et al, 2016). Soil characteristic curves parameters (pore size index, bubbling pressure, and residual water content) were derived from literature values (Rawls et al., 1982) and they are constant in whole area. Root cohesion values (Fig. 5d), at the depth chosen for the physical modelling with HIRESSS, were obtained taking into account vegetational maps (Carta delle serie di vegetazione d'Italia, Italian Ministry of the Environment and Protection of Land and Sea) and values from literature of root cohesion (Bischetti, 2009; Burylo et al., 2010; Vergani et el., 2013) that were calculated considering the Fiber Bundle Model (Pollen et al., 2004). The initial soil saturation was empirical defined based on antecedent rainfall analysis. Moreover, considering the lithological and land use maps the exposure rock mask (Fig. 5h) was prepared, so that HIRESSS model avoided the simulation on steep rock slopes areas. The parameters are showed in Table 2 for all lithological classes.

In the study area, the rainfall hourly data from 27 pluviometers were available, therefore it was necessary to spatially distribute them to generate 10x10 m cell size input raster to ensure the correct program operation. The rainfall data were elaborated applying the Thiessen's polygon methodology (Rhynsburger, 1973) modified to take into account the elevation. Thiessen's polygon methodology, in fact, allows us to divide a planar space in some regions, and to assign the regions to the nearest point feature. This approach defines an area around a point, where every location is nearer to this point than to all the others. Thiessen's polygon methodology do not consider the morphology of the area, so the alert Zone B was divided in three catchment areas and the polygons were calculated for each rain gauges considering the reference catchment basin (Fig. 5).

4 Results

The HIRESSS model provide day-by-day a maps of landslide occurrence probability. To check false positive for both the simulated events, the first day of simulation, characterized by the absence of rainfall, was analysed. The results showed that those pixels with a high landslide occurrence probability are unstable because of morphometric reasons, predominantly high slope angles. To remove these false positive, a numeric mask was applied. Using the GIS software commands, it was possible to calculate the number of pixels of the first simulation day with a trigger probability value greater than 80% and delete them (Fig. 6). The mask was then applied to the rest of landslide occurrence probability maps.

To evaluate the model performance both temporal and spatial validation were carried out. To perform a sound validation is necessary to have information on spatial and temporal location of landslides. In particular, the time of occurrence is very rarely known with hourly precision, and usually landslides are related to a rainstorm, without any more precise information on time of occurrence (Rossi et al., 2013). Concerning the spatial landslides locations, in many cases they are included in the database only as points without any information on the area involved. In our database, provided by the local authorities, landslides are points with information on the day of occurrence.

In general, for both events temporal validation shows that the daily highest probability of occurrence, computed by HIRESSS, correspond with the days with real landslide occurrence and with the most intense precipitation.

The results of the first simulated event (24 - 31 May 2008) are shown in Fig. 7. The failure probability in the whole area is less than 25% for the first four days (from 24 to 27 May 2008) (Fig. 7a). The rainfall intensity increased since 27 May, reaching the highest value on 29 May, when the precipitation value was around 100 mm in the eastern sector of study area.

The HIRESSS model well simulate this passage: the 28 May and 29 May 2008 landslide occurrence probability maps show a considerable increase of the probability of failure with maximum values around 90% at the East of alert Zone B (Fig. 7 b, c). In the following days rainfall intensity decreases, and also the probability slowly decreases, being anyway still high on 30 May 2008. Landslides reported in the database are dated 30 May and 31 May 2008 (Fig. 7d).

Concerning the second event (25 - 28 April 2009) landslide occurrence probability is less than 25% for the first two days (25 and 26 April 2009) in the whole area (Fig. 8 a, b), because of the low rainfall intensity. From 27 April 2009 rainfalls become more intense, especially in the southeast sector of the region, where the cumulated rainfall average was about 151 mm. This

event led to many landslides triggered during these days (as reported in the database). Also the probability maps show high values during these days (Fig. 8 c, d).

The temporal validation was also carried out considering daily cumulative rainfall compared to the landslide failure probability. In particular, a median of landslide occurrence probability was calculated for four pluviometric areas identified by Thiessen's polygons methodology, modified according to limits of river basins, both for the event of May 2008 and for the April 2009 event (Fig. 9 a, b). As it could be expected, the results show that when the highest rainfall intensity is measured, the highest probability of occurrence is computed for the all areas and for both events.

Spatial validation was performed following a pixel by pixel method: this method is the most complex since it consists in comparing the probability of instability of each pixel with the pixels involved in the actual event that occurred. This validation implies a great deal of uncertainty in the results since the reports of landslide events may have errors on the precise spatial location and on the size of the phenomenon. To overcome this problem and taking into account probable errors caused by the actual spatial location in the database, an area of 1 km^2 (called influence area) around the point of the landslide were considered in the validation analysis. Inside the influence area, pixels that have the 75% of probability of failure were considered instable.

Figure 10 shows an example of landslide event occurred in the Arnad municipality on 30 May 2008. The model computes a low failure probability on 24 May 2008 and an increase of probability on 30 May 2008. In Fig. 10 a and b it is possible to note that inside the red circle the red and yellow area increase on 30 May with respect to 24 May. In this case, the model is able to identify correctly such movement. To better highlight this validation, Figure 10c shows the number of pixels above 75% of probability calculated by the model, within the circular area of about 1 km^2 around the all landslides occurred during the event of 2008. For some of the reported landslide events, the number of pixels above 75% increases on 30 May,2008, only in case of the Champdepraz and Montjovet 2 events the probability does not increase. This may be caused by the low precision of location of the reported landslide, and maybe because some of the real landslides reported are other types of movements (rockfalls, rotational slides) that can not simulated by the HIRESSS model.

5 Discussion

The final aim of the physically-based modelling for landslide prediction is to set-up an early warning system at regional scale based on the model output. The validation of the results performed in the previous section showed that the HIRESSS model performs good results with good prediction capacity both from a spatial and temporal point of view. In this work the HIRESSS model computes the daily probability of occurrence with a spatial resolution of 10 m. In order to become an active and proficient early warning system it is necessary to define a method for the interpretation of the probabilistic results (e.g., definition of probability values corresponding to alert thresholds). Furthermore, in order to have more usable results especially for public administration and civil protection authorities it is necessary to possibly aggregate the model outputs temporally and spatially.

In particular, we selected a spatial aggregation method at the municipality level. Three level of failure probabilities (low, medium and high) are defined based on the expert-judged analysis of the cumulated frequency of the municipality median values of failure probability in the most critical day of the event (e.g., highest rainfall and failure probability). This procedure was done for the two events described in Sect. 4, defining for each of them different failure probability thresholds.

Once defined the three classes of probability, each municipality was classified according to the median value of probability inside its perimeter for each day. The results for the two analysed events are shown in Fig. 11 and Fig. 12. It is worth to notice that for some municipalities with the increase of rainfall intensity there is an increase of failure probabilities values from low (green) to red (high) that can be further translated in alert levels. The validation reported in Table 3 show the number of landslides for each failure class (low, medium high). It is worth noticing that for both events the majority landslides are located in the municipalities with low and medium HIRESSS probability of occurrence.

Figure 11 and Figure 12 are examples of how the model results can be analysed but the validation results are not satisfactory. The results have to be refined and the approach should be tailored to end users needs and requirements, in particular, the following aspects should be taken into account:

- spatial resolution: we have selected the municipality as spatial level of aggregation but also another types of spatial units (e.g., first or second order basins, Rossi et al., 2013) can be taken into account depending on the end-users needs and type of early warning system;
- temporal resolution: in this work HIRESSS has computed daily failure probabilities. The model is coded anyway to compute FS with different temporal resolutions. In real time applications the model can produce results with different time steps (e.g., six or twelve hours);
- definition of thresholds: the validation results show that the applied approach based on the analysis of cumulated median values of failure probabilities is not good enough to correctly forecast landslides. Different thresholds should be defined for each spatial unit of the early warning system based on a sound statistical analysis of HIRESSS results. To do a satisfactory analysis is necessary to have a good dataset of past triggered landslides.

6 Conclusion

The HIRESSS code (a physically-based distributed slope stability simulator for analysing shallow landslide triggering conditions in real time and in large areas) was applied to the eastern sector of Valle d'Aosta region in order to test its capability to forecast shallow landslides at regional scale. The model was applied in back analysis to two past rainfall events that have triggered in the study areas several shallow landslides between 2008 and 2009. The outcomes of the model are daily failure probability maps with a spatial resolution of 10 m. In order to run the model and to increase its reliability, an in-depth study of the geotechnical and hydrological properties of hillslopes controlling shallow landslides formation was conducted. In particular, two campaigns of on site measurements and laboratory experiments were performed with 12 survey points. The data collected contributes to generate input map of parameters for HIRESSS model. The effect of vegetation on

slope stability in terms of root reinforcement has been also taken into account based on the vegetation map and literature values producing a map of root cohesion. To evaluate the model performance both temporal and spatial validation were carried out, and in general for both the simulated events the computed highest daily probability of occurrence corresponds to the days and the areas of real landslides.

References

Reference List

Aleotti, P.: A warning system for rainfall-induced shallow failures, Eng. Geol., 73, 247–265, doi:10.1016/j.enggeo.2004.01.007, 2004.

Amoozegar, A.: Compact constant head permeameter for measuring saturated hydraulic conductivity of the vadose zone, Soil Sci. Soc. Am. J., 53, 1356–1361, 1989.

Arnone, E., Noto, L. V., Lepore, C., and Bras, R. L.: Physically- based and distributed approach to analyse rainfall-triggered land- slides at watershed scale, Geomorphology, 133, 3–4, 121–131, 2011.

Baum, R., Savage, W., and Godt, J.: Trigrs: A FORTRAN program for transient rainfall infiltration and grid-based regional slope- stability analysis, Open-file Report, US Geol. Survey, 2002.

Baum, R. L. and Godt, J. W.: Early warning of rainfall-induced shallow landslides and debris flows in the USA, Landslides, 7, 259–272, 2010.

Bicocchi, G., D'Ambrosio, M., Rossi, G., Rosi, A., Tacconi Stefanelli, C., Segoni, S., Nocentini, M., Vannocci, P., Tofani, V., Casagli N., and Catani, F.: Geotechnical in situ measures to improve landslides forecasting models: A case study in Tuscany (Central Italy), Landslides and Engineered Slopes, Experience, Theory and Practice, 2, 419–424, 2016.

Bischetti, G. B., Chiaradia, E. A., and Epis, T.: Prove di trazione su radici di esemplari di piante pratiarmati, Rapporto interno, Istituto di Idraulica Agraria, Università degli Studi di Milano, 2009.

Burylo, M.: Relations entre les traits fonctionnels des espèces végétales et leurs fonctions de protection contre l'erosion dans le milieu marneux restaurés de montagne, Dissertation, University of Grenoble, France, 2010.

Cannon, S. H., Boldt, E. M., Laber, J. L., Kean, J. W., and Staley, D. M.: Rainfall intensity–duration thresholds for postfire debris- flow emergency-response planning, Nat. Hazards, 59, 209–236, 2011.

Catani, F., Segoni, S., and Falorni, G.: An empirical geomorphology-based approach to the spatial prediction of soil thickness at catchment scale, Water Resour. Res., 46, W05508, doi:10.1029/2008WR007450, 2010.

Chirico, G. B., Borga M., Tarolli P., Rigon R., and Preti F.: Role of vegetation on slope stability un- der transient unsaturated conditions, Proced. Environ. Sci.,19, 932- 94, 2013.

De Giusti, F., Dal Piaz, G. V., Massironi, M., and Schiavo, A.: Carta geotettonica della Valle d'Aosta alla scala 1:150.000, Mem. Sci. Geol., 55, 129–149, 2004.

Del Soldato, M., Segoni, S., De Vita, P., Pazzi, V., Tofani, V., and Moretti, S.: Thickness model of pyroclastic soils along mountain slopes of Campania (southern Italy), In: Aversa, et al. (Eds.), Landslides and Engineered Slopes, Experience, Theory and Practice, Associazione GEotecnica Italaian, Rome, Italy, 797–804, 2016.

Dietrich, W. and Montgomery, D.: Shalstab: a digital terrain model for mapping shallow landslide potential, NCASI (National Coun- cil of the Paper Industry for Air and Stream Improvement) Technical Report, February, 1998.

Ennos, A. R.: The anchorage of Leek seedlings—the effect of root length and soil strength, Ann. Bot., 65, 409–416, 1990.

Giadrossich, F., Preti, F., Guastini, E., and Vannocci, P.: Metodologie sperimentali per l'esecuzione di prove di taglio diretto su terre rinforzate con radici, Experimental methodologies for the direct shear tests on soils reinforced by roots, Geologia tecnica & ambientale, 4, 5–12, 2010.

Gray, D. H., and Megahan, W. F.: Forest Vegetation Removal and Slope Stability in the Idaho Batholith, Forest Service, United States Department of Agriculture, Intermountain Forest and Range Experimental Station Research Paper INT-271, Boise, Idaho, 1–23, 1981.

Gray, D. H., and Ohashi, H.: Mechanics of fiber reinforcement in sand, J. Geotech. Eng., 109, 335–353, 1983.

Gray, D. H., and Sotir, R. B.: Biotechnical and Soil Bioengineering Slope Stabilization, John Wiley & Sons Inc., 378, 1996.

Greenway, D. R.: Vegetation and slope stability, In Slope Stability, Anderson MG, Richards KS (eds), Wiley, Chichester, 187–230 1987.

Intrieri, E., Gigli, G., Casagli, N., and Nadim, F.: Landslide early warning system: toolbox and general concepts. Nat. Hazard Earth Sys., 13, 85–90, 2013

Lagomarsino, D., Segoni, S., Fanti, R., and Catani, F.: Updating and tuning a regional scale landslide early warning system, Land- slides, 10, 91–97, 2013.

Lu, N. and Godt, J. W.: Infinite-slope stability under steady un- saturated seepage conditions, Water Resour. Res., 44, W11404, doi:10.1029/2008WR006976, 2008.

Martelloni, G., Segoni, S., Fanti, R., and Catani, F.: Rainfall thresh- olds for the forecasting of landslide occurrence at regional scale, Landslides, 9, 485–495, 2012.

Mercogliano, P., Segoni, S., Rossi, G., Sikorsky, B., Tofani, V., Schiano, P., Catani, F., and Casagli, N.: Brief communication "A prototype forecasting chain for rainfall induced shallow landslides", Nat. Hazards Earth Syst. Sci., 13, 771–777, doi:10.5194/nhess-13-771-2013, 2013.

Operstein, V., and Frydman, S.: The influence of vegetation on soil strength, Ground. Improv., 4, 81–89, 2000.

Pack, R. T., Tarboton, D. G., and Goodwin, C. N.: Assessing terrain stability in a gis using sinmap, in "15th Annual GIS Conference, GIS 2001, Vancouver, British Columbia, Canada, 2001.

Park, H. J., Lee, J. H. and Woo, I.: Assessment of rainfall-induced shallow landslide susceptibility using a GIS-based probabilistic approach, Eng. Geol., 161, 1–15, 2013.

Pollen, N., Simon, A., and Collison, A. J. C.: Advances in assessing the mechanical and hydrologic effects of riparian vegetation on streambank stability, in Riparian Vegetation and Fluvial Geomorphology, Water Sci. Appl. Ser., 8, edited by Bennett, S., and Simon, A., AGU, Washington, D. C., 125–139, 2004.

Rawls, W. J., Brakensiek, D. L., and Saxton K. E.: Estimating soil water properties, Transactions, ASAE, 25(5),1316–1320 and 1328 1982.

Ren, D., Fu, R., Leslie, L. M., Dickinson, R. and Xin X.: A storm-triggered landslide monitoring and prediction system: formulation and case study, Earth Interact., 14,1–24, 2010.

Rhynsburger, D.: Analytic delineation of Thiessen polygons, Geogr. Anal., 5(2), 133–144, 1973.

Richards, L. A.: Capillary conduction of liquids through porous mediums, PhD Thesis, Cornell University, 1931.

Rosi, A., Segoni, S., Catani, F., and Casagli, N.: Statistical and envi- ronmental analyses for the definition of a regional rainfall thresholds system for landslide triggering in Tuscany (Italy), J. Geogr. Sci., 22, 617–629, 2012.

Rossi, G., Catani, F., Leoni, L., Segoni, S., and Tofani, V.: HIRESSS: a physically based slope stability simulator for HPC applications, Nat. Hazards Earth Syst. Sci., 13, 151–166, doi:10.5194/nhess-13-151-2013, 2013.

Salciarini, D., Tamagnini, C., Conversini, P., and Rapinesi, S.: Spatially distributed rainfall thresholds for the initiation of shallow landslides, Nat. Hazards, 61(1), 229–245, doi:10.1007/s11069-011-9739-2, 2012.

Salciarini, D., Fanelli, G., Tamagnini, C.: A probabilistic model for rainfall-induced shallow landslide prediction at the regional scale, Landslides, 14(5),1731–1746, 2017.

Simoni, S., Zanotti, F., Bertoldi, G., and Rigon, R.: Modelling the probability of occurrence of shallow landslides and channelized debris flows using GEOtop-FS, Hydrolog. Process., 22, 532–545, 2008.

Tofani, V., Bicocchi, G., Rossi, G., Segoni, S., D'Ambrosio, M., Casagli, N., and Catani, F.: Soil characterization for shallow landslides modeling: a case study in the Northern Apennines (Central Italy), Landslides, 14, 755–770, doi: 10.1007/s10346-017-0809-8, 2017.

UNISDR: "UN/ISDR terminology on disaster risk reduction", UN/ISDR Library on disaster risk reduction, UN/ISDR, Nairobi, available at: www.unisdr.org/eng/library/ lib-terminology-eng.htm, 2009.

Vergani, C., Giadrossich, F., Schwarz, M., Buckley, P., Conedera, M., Pividori, M., Salbitano, F., Rauch, H. S., and Lovreglio, R.: Root reinforcement dynamics of European coppice woodlands and their effect on shallow landslides, a review Earth Sci. Rev., 167, 88–102, doi:10.1016/j.earscirev.2017.02.002, 2017.

Vergani, C., Bassanelli, C., Rossi, L., Chiaradia, E. A., and Bischetti, G. B.: The effect of chestnut coppice forest abandon on slope stability: a case study, Geophys. Res Abstr, 15, EGU2013-10151, 2013.

Wagner, A. A.: The use of the Unified Soil Classification System by the Bureau of Reclamation, Proc. 4th Intern. Conf. Soil Mech. Found. Eng., London, 1, 125, 1957.

Waldron, L. J.: The shear resistance of root-permeated homogenous and stratified soil, Soil Sci. Soc. Am. J. 41,843–849, 1977.

Waldron, L. J., and Dakessian, S.: Soil reinforcement by roots: calculations of increased soil shear resistance from root properties, Soil Sci., 132, 427–435,1981.

Nat. Hazards Earth Syst. Sci. Discuss., https://doi.org/10.5194/nhess-2017-425
Manuscript under review for journal Nat. Hazards Earth Syst. Sci.
Discussion started: 2 January 2018

Natural Hazards and Earth System Sciences
Discussions

Table 1. Geotechnical properties of survey points (grain size distribution, Atterberg limits, index properties, permeability and shear strength parameters).

SITE	*SOIL TYPE*	*G %*	*S %*	*M %*	*C %*	*LL (%)*	*PL (%)*	*PI (%)*	*USCS*	*γ (kN m^{-3})*	*γ_d (kN m^{-3})*	*γ_{sat} (kN m^{-3})*	*n (%)*	*w (%)*	*k_s (m s^{-1})*	*k_{sc} (m s^{-1})*	*ϕ' lab (°)*	*c' (kPa)*
Site 1	Sand with silty gravel	27.8	45.2	23.4	3.6	36	25	11	SM	16.7	13.7	18.3	47.3	11.3	/	2.52E-06	25.6	1.0
Site 2	Sand with gravelly silt	19.4	50.5	29.0	1.1	38	25	14	SC	19.1	14.5	18.8	44.3	11.4	2.71E-06	1.48E-06	34.3	1.5
Site 3	Sand with gravel and silt	26.9	45.2	26.8	1.1	/	/	/	/	/	/	/	/	/	/	8.89E-07	/	/
Site 4	Sand with gravelly silt	18.8	40.4	39.2	1.6	38	27	11	SM	19.5	14.8	19.0	43.2	10.7	1.36E-07	4.51E-07	34.3	0.0
Site 5	Sand with gravel and silt	31.0	43.1	25.7	0.2	47	36	11	SM	18.4	14.0	18.5	46.3	11.0	/	2.44E-06	25.7	9.3
Site 6	Sand with poorly silty gravel	28.5	57.5	13.9	0.1	52	38	13	SM	18.7	13.5	18.2	47.9	20.0	/	8.27E-06	30.2	4.4
Site 7	Sand with silty gravel	37.0	42.6	17.9	2.5	40	32	8	SM	20.3	15.5	19.5	40.4	26.2	5.18E-06	2.97E-06	28.2	3.4
Site 8	Sandy silty gravel	58.1	24.6	16.0	1.3	43	28	16	GM	17.2	15.7	19.6	39.6	9.4	/	3.76E-06	30.1	8.1
Site 9	Gravelly silty sand	18.7	55.1	24.4	1.8	46	36	10	SM	20.1	18.7	21.5	27.9	8.1	2.41E-06	1.73E-06	33.9	0.6
Site 10	Sand with gravelly silt	21.9	52.0	25.1	1	46	37	8	SM	18.4	16.0	19.8	38.6	15.5	/	2.10E-06	30.3	1.5
Site 11	Gravelly silty sand	24.3	51.4	21.2	3.1	31	25	7	SM	21.7	18.0	21.2	31.9	20.5	4.03E-06	3.05E-06	29.8	2.0
Site 12	Gravel with poorly silty sand	55.2	32.2	12.2	0.4	55	45	10	SM	15.3	14.6	18.9	43.9	5.1	1.54E-05	8.25E-06	30.2	1.6
	MEAN	30.63	44.98	22.9	1.48	42.91	32.18	10.82		18.67	15.36	19.39	41.03	13.56	4.98E-06	3.16E-06	30.24	3.04
	MEDIAN	27.35	45.2	23.9	1.2	43	32	11		18.7	14.8	19.0	43.2	11.3	3.37E-06	2.48E-06	30.2	1.6
	STD.DEV	13.31	9.48	7.41	1.11	7.15	6.71	2.71	/	1.80	1.68	1.10	6.34	6.30	5.38E-06	2.56E-06	3.05	3.07
	MAX	58.1	57.5	39.2	3.6	55	45	16		21.7	18.7	21.5	47.9	26.2	1.54E-05	8.27E-06	34.3	9.3
	MIN	18.7	24.6	12.2	0.1	31	25	7		15.3	13.5	18.2	27.9	5.1	1.36E-07	4.51E-07	25.6	0

Nat. Hazards Earth Syst. Sci. Discuss., https://doi.org/10.5194/nhess-2017-425
Manuscript under review for journal Nat. Hazards Earth Syst. Sci.
Discussion started: 2 January 2018

Natural Hazards and Earth System Sciences
Discussions

Table 2. Geotechnical parameters of each lithological class as input for HIRESSS model.

Lithological classes	*Soil Type*	*ϕ' lab (°)*	*c' (Pa)*	*γ_d (kN m^{-3})*	*n (%)*	*k_s (m s^{-1})*	*h_s*	*q_r*	*l*
Calcareous schist	Sand with gravelly silt	31	1000	16.5	39	1.1E-05	0.1466	0.041	0.322
Alluvial deposits	Sand with gravel and silt	26	1000	14.0	46	3.0E-06	0.1466	0.041	0.322
Glacial deposits	Sand with silty gravel	31	1000	15.3	41	2.7E-06	0.1466	0.041	0.322
Colluvial deposits	Sand with silty gravel	25	1000	13.7	47	2.5E-06	0.1466	0.041	0.322
Granites	Sandy gravel	30	1000	17.6	32	4.0E-06	0.1466	0.041	0.322
Mica schists	Sandy silty gravel	30	1000	17.7	32	6.0E-06	0.1466	0.041	0.322
Pietre Verdi	Gravel with silty sand	32	1000	16.3	37	4.6E-06	0.1466	0.041	0.322

Table 3. The number of landslides for each failure class.

Failure probability	29 May 2008	27 April 2009
Low	5	4
Medium	4	6
High	0	1

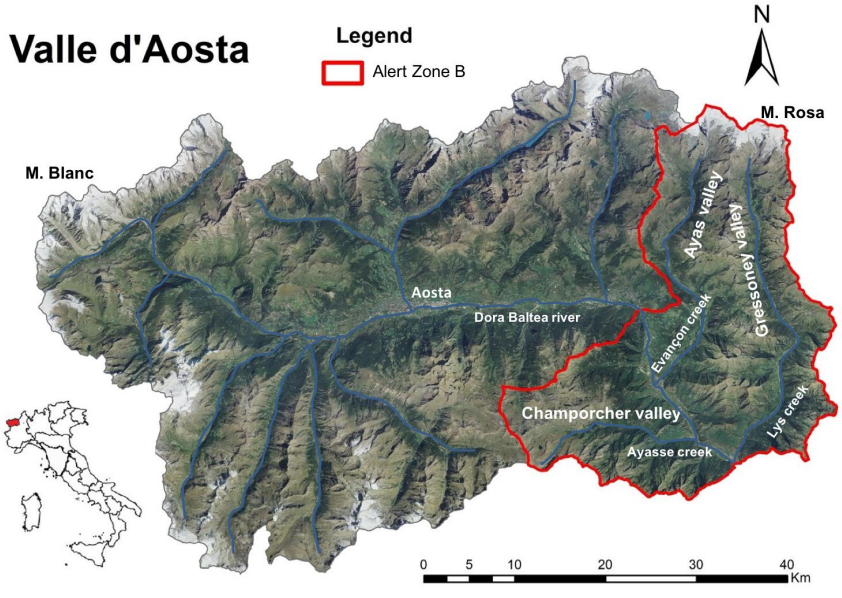

Figure 1. Valle d'Aosta region in the NW Italy: in red the study area, alert Zone B.

Nat. Hazards Earth Syst. Sci. Discuss., https://doi.org/10.5194/nhess-2017-425
Manuscript under review for journal Nat. Hazards Earth Syst. Sci.
Discussion started: 2 January 2018

Natural Hazards and Earth System Sciences
Discussions

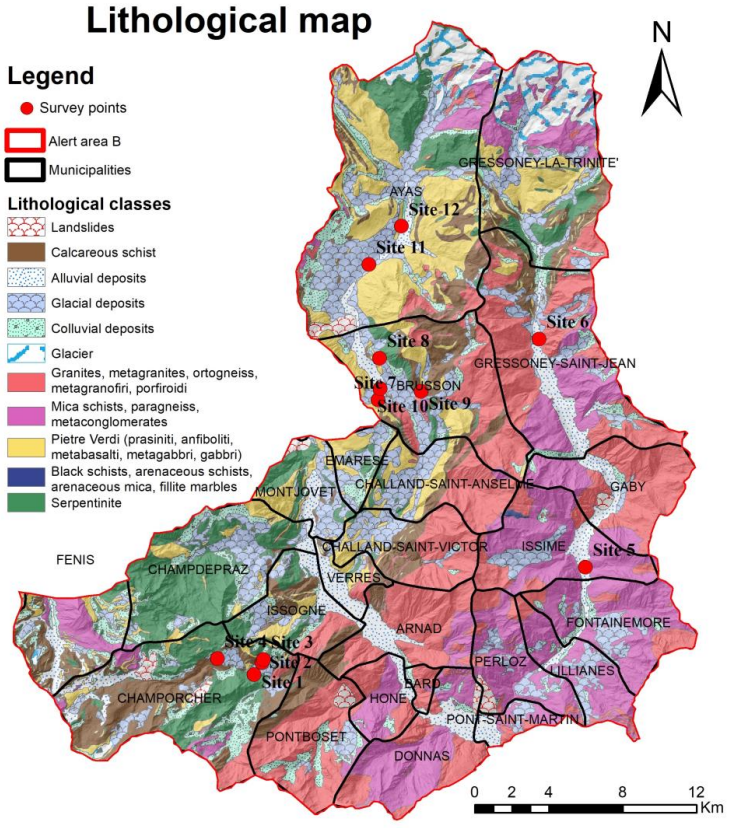

Figure 2. Spatial distribution of survey points compared to the geo-lithology.

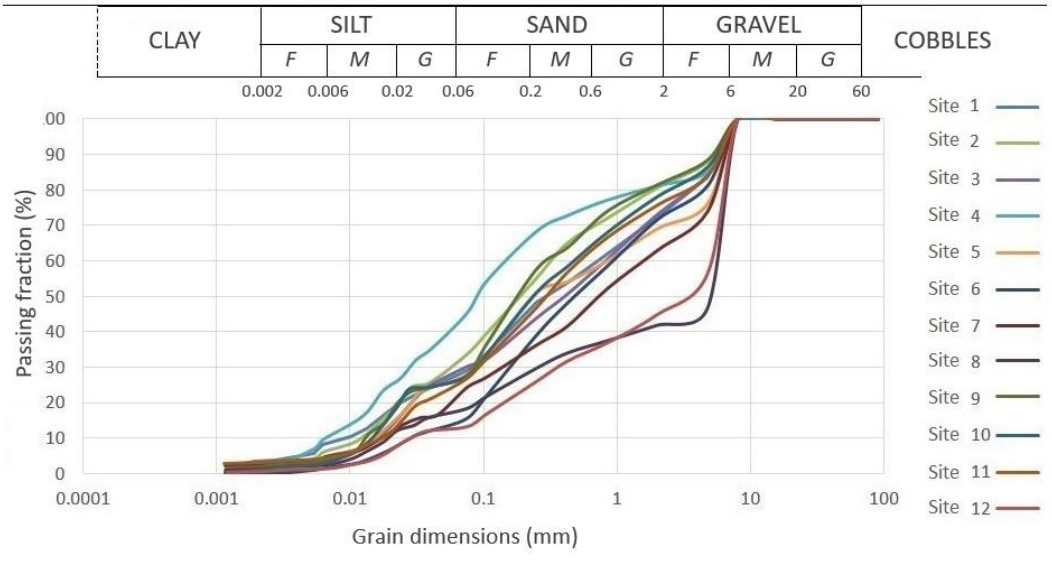

Fig 3. Grain size distributions.

Nat. Hazards Earth Syst. Sci. Discuss., https://doi.org/10.5194/nhess-2017-425
Manuscript under review for journal Nat. Hazards Earth Syst. Sci.
Discussion started: 2 January 2018

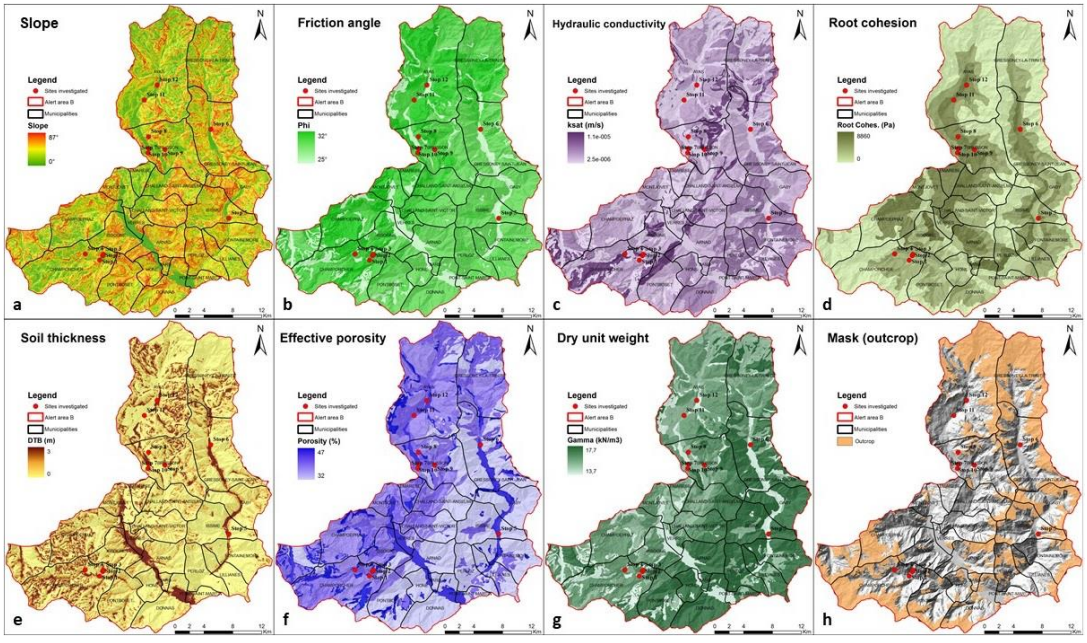

Figure 4. Static input parameters for HIRESSS model, a) slope gradient; b) root cohesion; c) friction angle; d) Hydraulic conductivity; e) soil thickness; f) effective porosity; g) dry unit weight; and h) exposure rock mask.

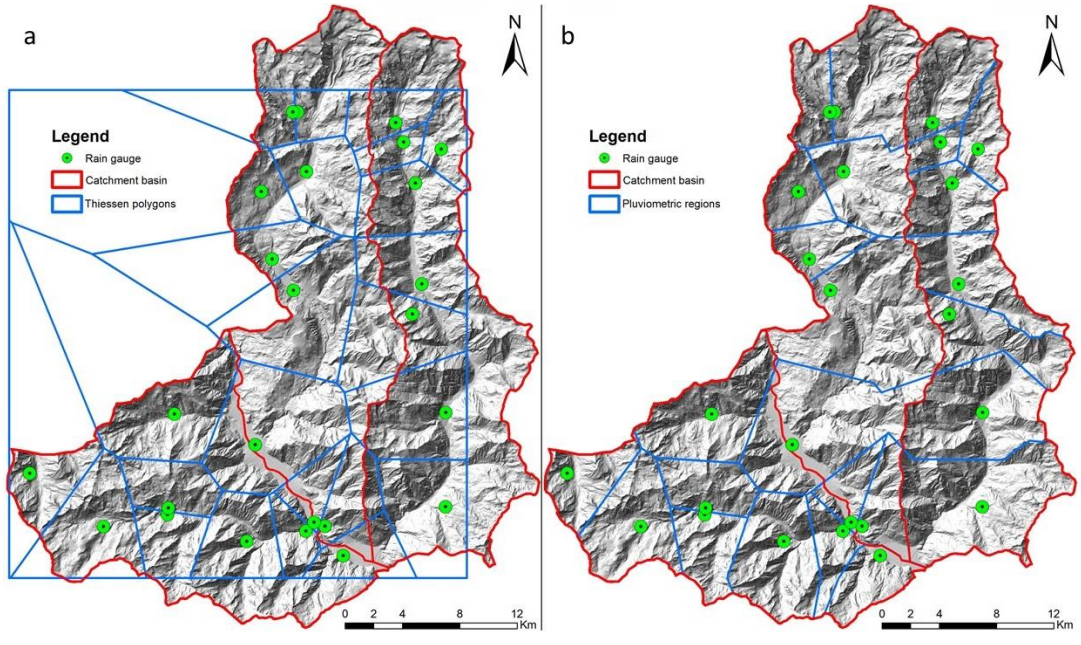

Figure 5. Comparison of Thiessen's polygons methodology a) simple b) modified according to the catchment basins boundaries.

Nat. Hazards Earth Syst. Sci. Discuss., https://doi.org/10.5194/nhess-2017-425
Manuscript under review for journal Nat. Hazards Earth Syst. Sci.
Discussion started: 2 January 2018

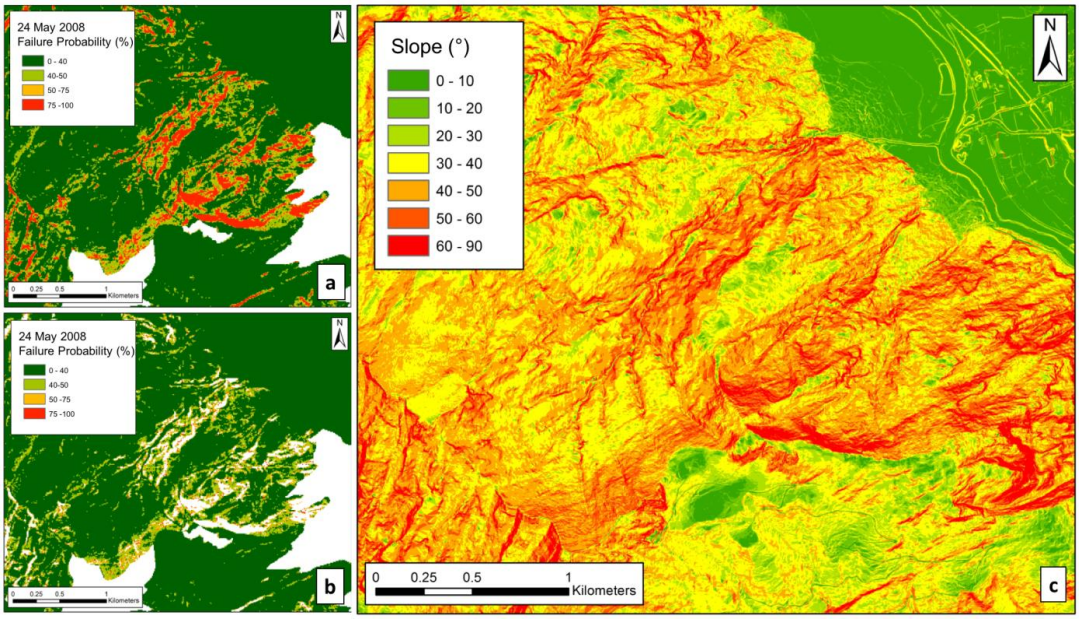

Figure 6. Example of numerical mask to remove the false positive of the first event simulated, between 24-31 May 2008, a) the HIRESSS result of the first day of simulation with false positive pixels, b) the probability map after the numerical mask implementation, c) the slope map shows that the pixels with high probability of landslide occurrence are located where the slope is higher than 60%.

Nat. Hazards Earth Syst. Sci. Discuss., https://doi.org/10.5194/nhess-2017-425
Manuscript under review for journal Nat. Hazards Earth Syst. Sci.
Discussion started: 2 January 2018

Natural Hazards and Earth System Sciences
Discussions

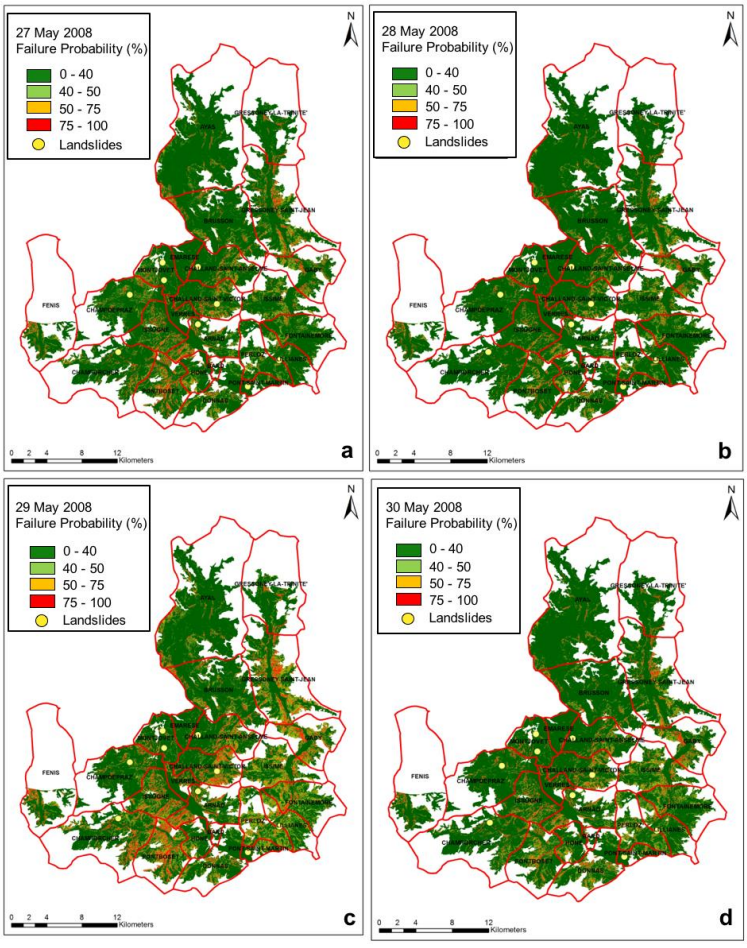

Figure 7. HIRESSS landslide probability maps of simulate event of 24-31 May 2008 and reporting landslide during this event focused on the four critical days, a) 27 May 2008, b) 28 May 2008, c) 29 May 2008, and d) 30 May 2008.

Nat. Hazards Earth Syst. Sci. Discuss., https://doi.org/10.5194/nhess-2017-425
Manuscript under review for journal Nat. Hazards Earth Syst. Sci.
Discussion started: 2 January 2018

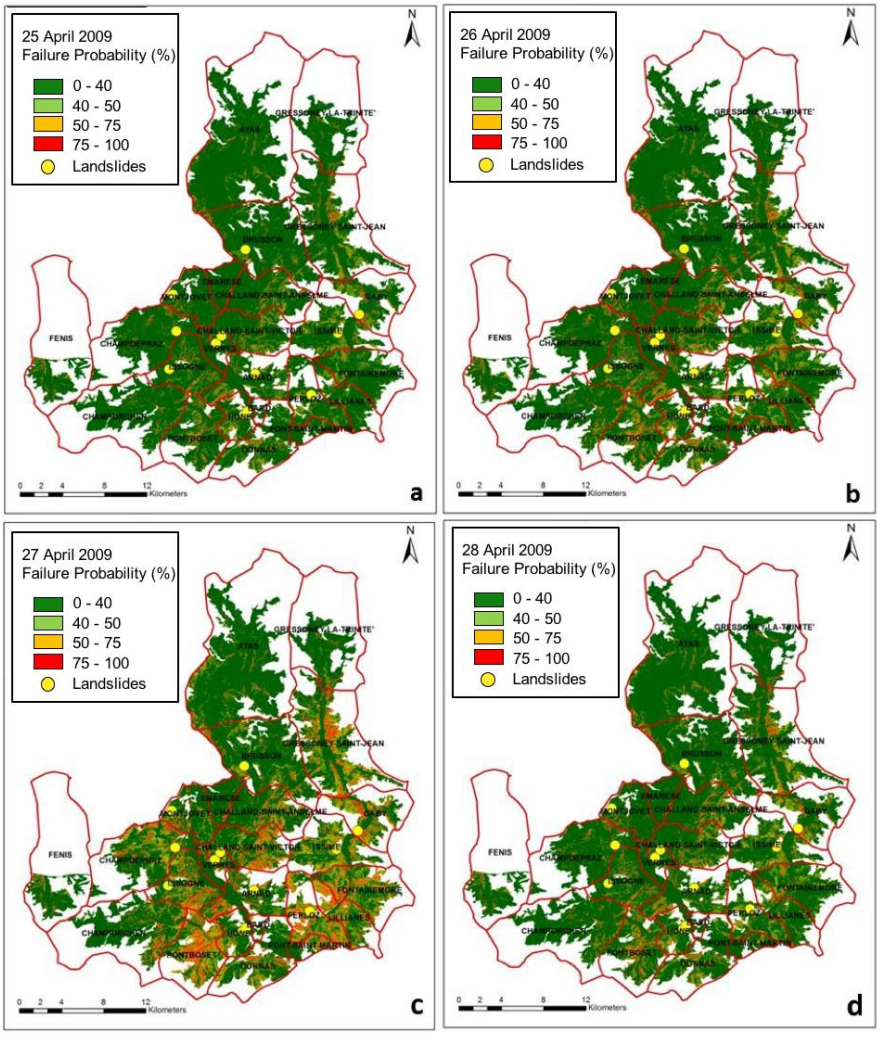

Figure 8. HIRESSS landslide probability maps of simulate event between 25 - 28 April 2009 and reporting landslide during this event, a) 25 April 2009, b) 26 April 2009, c) 27 April 2009 and d) 28 April, 2009.

Nat. Hazards Earth Syst. Sci. Discuss., https://doi.org/10.5194/nhess-2017-425
Manuscript under review for journal Nat. Hazards Earth Syst. Sci.
Discussion started: 2 January 2018

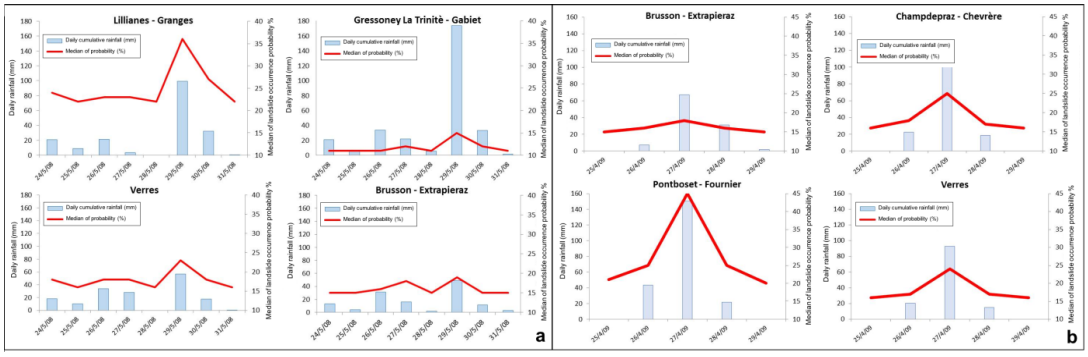

Figure 9. Correlation graphs between the daily cumulative rainfall and the median of landslide occurrence probability for both events.

5

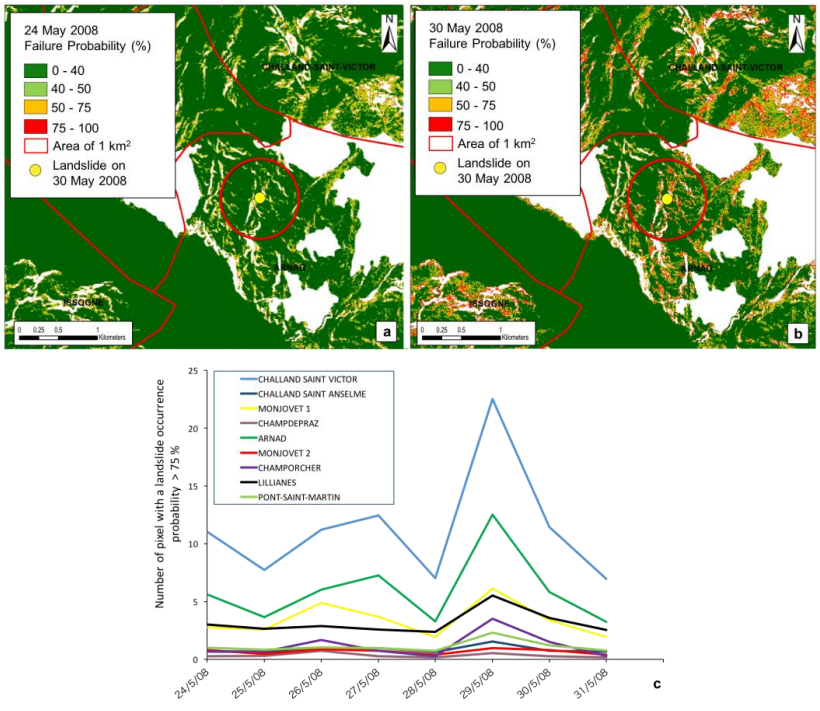

Figure 10. An example of landslide event happened in the Arnad municipality compared to landslide occurrence probability map, a) before and b) after rainfall event. c) Number of pixels above 75% of probability calculated by the model for all the landslides triggered during the event in the study area.

Nat. Hazards Earth Syst. Sci. Discuss., https://doi.org/10.5194/nhess-2017-425
Manuscript under review for journal Nat. Hazards Earth Syst. Sci.
Discussion started: 2 January 2018

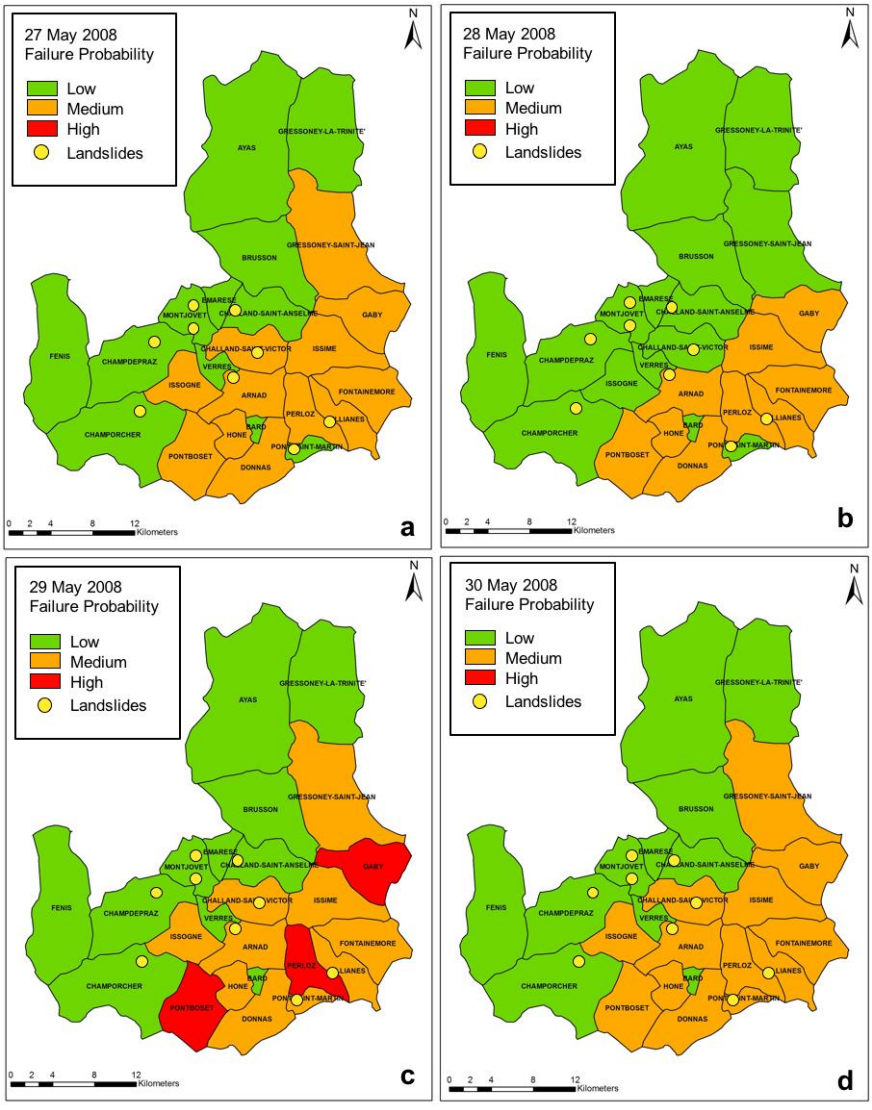

Figure 11. Spatial aggregation method at the municipality level for the events of May 2008 according to the value of failure probability.

Nat. Hazards Earth Syst. Sci. Discuss., https://doi.org/10.5194/nhess-2017-425
Manuscript under review for journal Nat. Hazards Earth Syst. Sci.
Discussion started: 2 January 2018

Natural Hazards and Earth System Sciences
Discussions

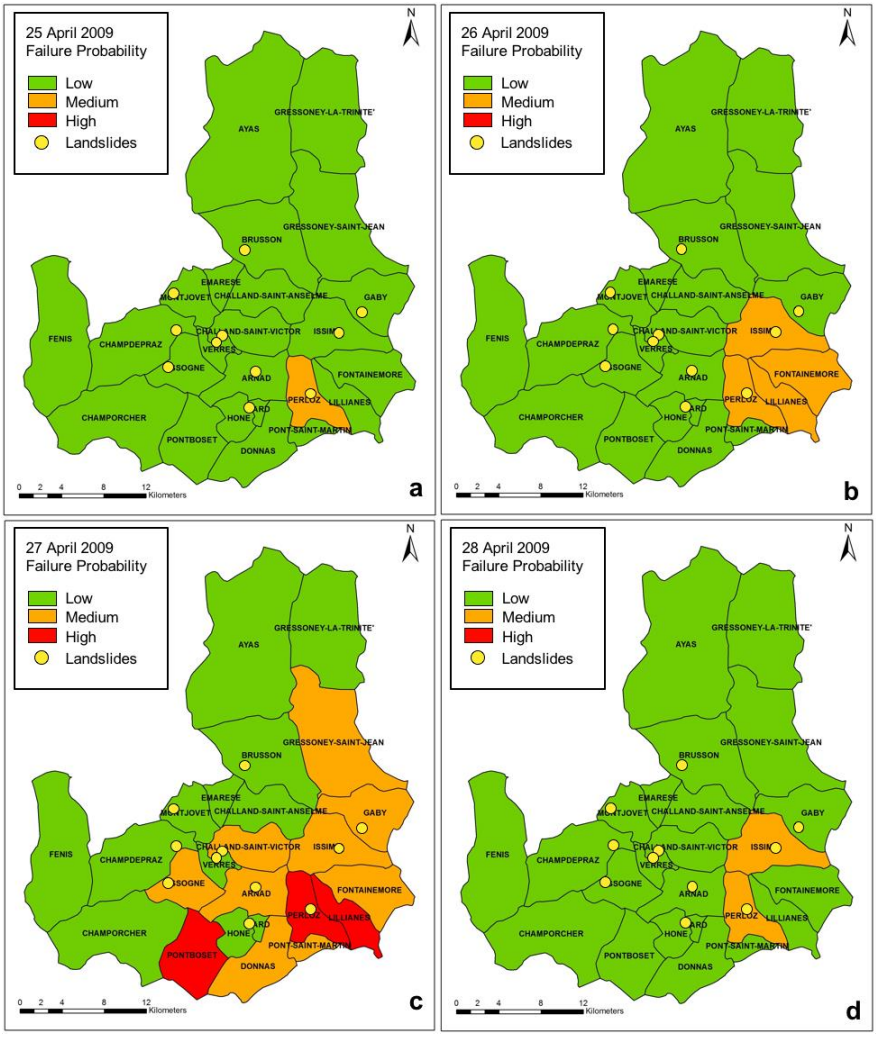

Figure 12. Spatial aggregation method at the municipality level for the events of April 2009 according to the value of failure probability.